Inorg. Chem. **2007**, *46*, 4583–4591

Rich Pseudopolymorphic Behavior of the Tetranuclear $[Ni_4(dpyatriz)_2(NO_3)_8]$ Complex

Hélène Casellas,[†] Olivier Roubeau,[‡] Simon J. Teat,[§] Norberto Masciocchi,*[,||] Simona Galli,[||] Angelo Sironi,[⊥] Patrick Gamez,*[,†] and Jan Reedijk[†]

Leiden Institute of Chemistry, PO Box 9502, 2300 RA Leiden, The Netherlands, Centre de Recherche Paul Pascal-CNRS UPR 8641, 115 avenue du dr. A. Schweitzer, 33600 Pessac, France, ALS, Berkeley Lab, 1 Cyclotron Rd, MS2-400, Berkeley, California 94720, Dipartimento di Scienze Chimiche e Ambientali, Università dell'Insubria, via Valleggio 11, I-22100 Como, Italy, and Dipartimento di Chimica Strutturale e Stereochimica Inorganica, Università di Milano, via Venezian 21, I-20133 Milano, Italy

Received February 4, 2007

Reaction of nickel(II) nitrate with the dpyatriz ligand, namely 2,4,6-tris(bis(pyridin-2-yl)amino)-1,3,5-triazine, in acetonitrile produces a tetranuclear Ni^{II} coordination compound, $[Ni_4(dpyatriz)_2(NO_3)_8(CH_3CN)_2(H_2O)_2]\cdot 2CH_3CN$ (**1**), the crystal structure of which has been determined by X-ray diffraction using a synchrotron source. **1** has been characterized by IR and UV–vis spectroscopy, elemental and thermogravimetric analyses, and magnetic susceptibility measurements. Its solid-state structure exhibits remarkable anion$\cdots\pi$ interactions between coordinated nitrate ions and the triazine rings. In addition, a thorough X-ray powder diffraction study has revealed a number of pseudopolymorphic phases (**2**–**5**), resulting from various degrees of hydration/solvation of the $[Ni_4(dpyatriz)_2]$ core. The interconversion scheme among the different phases has been determined using controlled heating, and the basic structural features of the different pseudopolymorphs have been assessed through ab initio powder diffraction methods.

Introduction

Polymorphism is the ability of a solid material to exist in at least two different crystal packing arrangements.[1,2] Pseudopolymorphism defines the aptitude of a crystalline compound to form solvates or hydrates through the incorporation of respectively an organic solvent or water into the lattice of the solid-state structure.[3,4] The potential existence of various pseudopolymorphic forms for the same compound, associated with the consequent distinct physical properties, has been recognized and properly addressed, especially for pharmaceutical applications.[5,6] Indeed, the insertion of water molecules in a drug substance may lead to metastable or amorphous phases, decreasing its chemical and/or physical stability.[7,8] In addition, its density, solubility, dissolution rate, or bioavailability may also be affected.[9] Therefore, an important topic of investigation in crystal engineering is to study the formation of pseudopolymorphs and examine their physical properties.

During the past 5 years, we have been involved in the preparation of coordination compounds featuring the 1,3,5-triazine ring.[10] The 1,3,5-triazine (also known as *s*-triazine)

* To whom correspondence should be addressed. E-mail: p.gamez@chem.leidenuniv.nl (P.G.), norberto.masciocchi@uninsubria.it (N.M.). Phone: +31715274260 (P.G.). Fax: +31715274671 (P.G.).
[†] Leiden Institute of Chemistry.
[‡] Centre de Recherche Paul Pascal-CNRS UPR 8641.
[§] ALS, Berkeley Lab.
[||] Università dell'Insubria.
[⊥] Università di Milano.

(1) Bilton, C.; Howard, J. A. K.; Madhavi, N. N. L.; Nangia, A.; Desiraju, G. R.; Allen, F. H.; Wilson, C. C. *Chem. Commun.* **1999**, 1675–1676.
(2) Pfeffer-Hennig, S.; Piechon, P.; Bellus, M.; Goldbronn, C.; Tedesco, E. *J. Therm. Anal. Calorim.* **2004**, *77*, 663–679.
(3) Brown, P. O.; Enright, G. D.; Ripmeester, J. A. *Cryst. Growth Des.* **2006**, *6*, 719–725.
(4) Alshahateet, S. F.; Bishop, R.; Craig, D. C.; Scudder, M. L.; Ung, A. T. *Struct. Chem.* **2001**, *12*, 251–257.
(5) Khankari, R. K.; Grant, D. J. W. *Thermochim. Acta* **1995**, *248*, 61–79.
(6) Kristl, A.; Srcic, S.; Vrecer, F.; Sustar, B.; Vojnovic, D. *Int. J. Pharm.* **1996**, *139*, 231–235.
(7) de Matas, M.; Edwards, H. G. M.; Lawson, E. E.; Shields, L.; York, P. *J. Mol. Struct.* **1998**, *440*, 97–104.
(8) Kim, Y. S.; Paskow, H. C.; Rousseau, R. W. *Cryst. Growth Des.* **2005**, *5*, 1623–1632.
(9) Kumar, V. S. S.; Pigge, F. C.; Rath, N. P. *Cryst. Growth Des.* **2004**, *4*, 1217–1222.
(10) Gamez, P.; Reedijk, J. *Eur. J. Inorg. Chem.* **2006**, 29–42.

10.1021/ic0702015 CCC: $37.00
Published on Web 04/18/2007

Chart 1. 2,4,6-Tris(bis(pyridin-2-yl)amino)-1,3,5-triazine (dpyatriz)

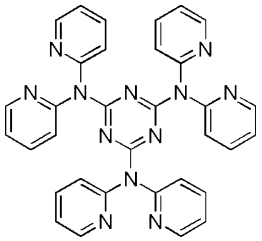

moiety is a prime building unit to generate intricate coordination networks with remarkable supramolecular characteristics. One specific supramolecular feature of this electron-deficient aromatic ring is its potential interaction with an anion.[11,12] "Anion−π" interactions are unconventional supramolecular contacts,[13] which have been mainly theoretically investigated.[14−16] Recently, in the course of synthetic efforts aimed at developing triazine-based anion−host systems, an interesting host−guest material capable of reversibly binding water guests in its host lattice, via the formation of a pseudopolymorphic hydrate, has been described.[17]

In this paper, the preparation and characterization of a tetranickel(II) complex of $[Ni_4(dpyatriz)_2(NO_3)_8(CH_3CN)_2(H_2O)_2]\cdot 2CH_3CN$ formula, **1** (dpyatriz = 2,4,6-tris(bis(pyridin-2-yl)amino)-1,3,5-triazine, Chart 1),[18,19] showing "anion−π" interactions, is reported. In addition, the amazing existence of at least five pseudopolymorphic forms, rising from different degrees of hydration/solvation of the $[Ni_4(dpyatriz)_2]$ core, has been revealed by a thorough X-ray powder diffraction study.

To facilitate the comprehension of this article, Chart 2 reports the complete formulas, the numbering scheme, and a summary of the interconversion processes observed among the five different pseudopolymorphs.

Experimental Section

General Remarks. All chemicals were of reagent grade and were used as commercially obtained. The ligand 2,4,6-tris(bis(pyridin-2-yl)amino)-1,3,5-triazine (Chart 1; dpyatriz) was synthesized according to a reported procedure.[18] Elemental analyses for C, H, and N were performed with a Perkin-Elmer 2400 analyzer. FTIR spectra were recorded with a Perkin-Elmer Paragon 1000 FTIR spectrophotometer, equipped with a Golden Gate ATR device, using the reflectance technique (4000−300 cm^{-1}). Ligand-field spectra were recorded on a Perkin-Elmer Lambda 900 spectrophotometer over the range 2000−200 nm, using the diffuse reflectance technique, with MgO as a reference. Thermogravimetric (TG) analyses were performed on a Perkin-Elmer Series 7 equipment, under nitrogen, at a heating rate of 10 °C min^{-1}. Magnetic susceptibility measurements (5−300 K) were carried out using a Quantum Design MPMS-5S SQUID magnetometer at 1000 Oe. Data were corrected for the diamagnetic contributions estimated from the Pascal constants.[20] The specific surface area of **3** was determined (single-point method) using a ThermoQuest analyzer (Italy).

Synthesis of $[Ni_4(dpyatriz)_2(NO_3)_8(CH_3CN)_2(H_2O)_2]\cdot 2CH_3CN$ (1). $Ni(NO_3)_2\cdot 6H_2O$ (29.8 mg, 0.10 mmol) was added to a suspension of dpyatriz (20 mg, 0.034 mmol) in acetonitrile (5 mL). The resulting clear blue solution was allowed to stand at 100 °C in a sealed Pyrex tube under autogenous pressure. Tiny cubic-shaped blue single crystals, suitable for X-ray diffraction, were obtained after 15 h and were formulated as $[Ni_4(dpyatriz)_2(NO_3)_8(CH_3CN)_2(H_2O)_2]\cdot 2CH_3CN$ (**1**). Anal. Calcd for $C_{74}H_{64}N_{36}Ni_4O_{26}$ (**1**) (fw = 2108.45): C, 42.16; H, 3.06; N, 23.92. Anal. Found (within 2 days from isolation from the mother liquors): C, 39.06; H, 2.84; N, 21.92. Found (later): C, 37.88; H, 3.84; N 21.83. Actually, **1** is extremely sensitive to air moisture. Thus, crystals of **1** are stable in the mother liquor at room temperature, but they immediately lose their shiny surface once they are filtered. A blue-gray powder is rapidly and quantitatively formed in contact with air. From the experimental C, H, and N analyses aforementioned, two compounds are sequentially formed. Compound **2** can be formulated as $[Ni_4(dpyatriz)_2(NO_3)_8(H_2O)_6]$. Anal. Calcd for $C_{66}H_{60}N_{32}Ni_4O_{30}$ (**2**) (fw = 2016.10): C, 39.32; H, 3.00; N, 22.23. Compound **3** is formulated as $[Ni_4(dpyatriz)_2(NO_3)_8(H_2O)_{12}]$. Anal. Calcd for $C_{66}H_{72}N_{32}Ni_4O_{36}$ (**3**) (fw = 2124.18): C, 37.32; H, 3.41; N, 21.10. These observations are in complete agreement with our XRPD studies (see Results and Discussion), which showed the intermediacy of the metastable compound **2**, which contains only six water molecules, during the **1** → **3** transformation. Main IR absorption bands for **3** (cm^{-1}): 3324, 1607, 1556, 1550, 1374, 1278, 1024, 818, 667, 435. UV−

Chart 2. Synoptic Collection of the Five Species Presented in the Text and of Their Interconversion Paths

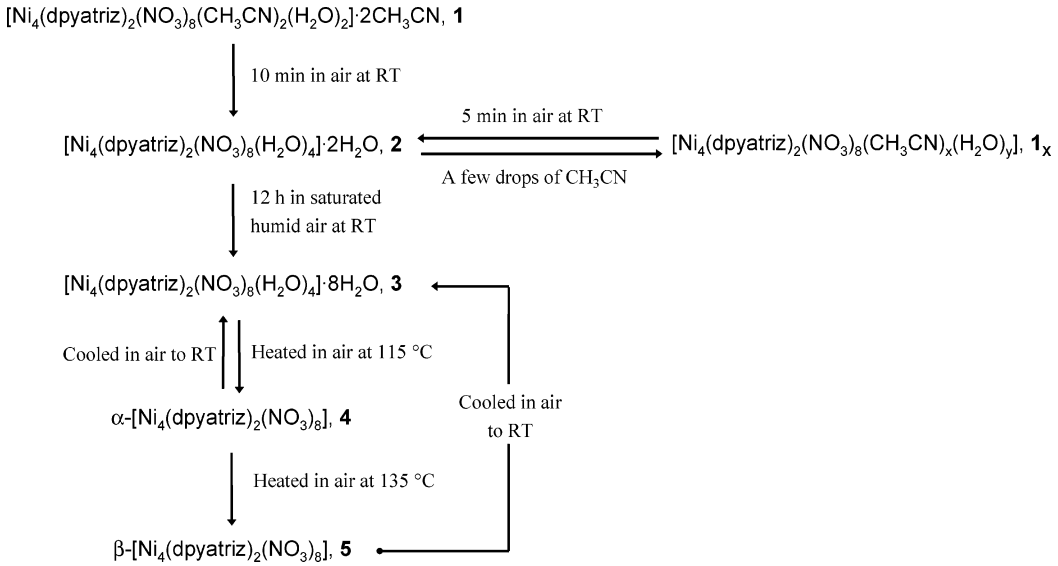

vis (reflectance, nm): 275, 381 (small), 453 (small), 589. Magnetic measurements show that there are no particular interactions in **3**, even at low temperatures. TG analysis: 10% weight loss between 20 and 130 °C, which is the value expected for the loss of 12 molecules of water by **3**. The specific surface area for **3** is 6 $m^2 g^{-1}$.

Crystallographic Analysis. Single-Crystal X-ray Diffraction Analysis for 1. A tiny single-crystal of **1** of size approximately $0.14 \times 0.08 \times 0.06$ mm^3 was selected for the X-ray measurements and mounted onto the diffractometer at ca. 150 K. The measurements were made using Si(111) monochromated synchrotron radiation ($\lambda = 0.6894$ Å) and a Bruker APEX II CCD diffractometer using standard procedures and programs for Station 9.8 of Daresbury SRS.[21] The intensity data were processed using SAINT v7.06a.[22] The structure was solved using direct methods with the SHELXTL program package.[23,24] All non-hydrogen atoms were refined anisotropically. Displacement and geometrical restraints were used in modeling the disordered nitrates. The hydrogen atoms were placed geometrically, where possible, or found in the difference map in the case of the clathrated acetonitrile. It was not possible to find or geometrically place those on the bound acetonitrile or the water molecules, and therefore, they were omitted form the final list of atoms. Hydrogen atoms were refined using a riding model. The highest peak in the difference map is located next to one of the nickel ions and is of 2 e/Å.^{3} The function minimized was $[w(F_o^2 - F_c^2)]$ with reflection weights $w^{-1} = [2F_o^2 + (g_1P)^2 + (g_2P)]$, where $P = [\max F_o^2 + 2F_c^2]/3$. Details of the X-ray single-crystal analysis refinement are listed in Table 1.

X-ray Powder Diffraction Analyses of 2−5. Diffraction data were recorded on a Bruker AXS D8 Advance diffractometer operating in the θ:θ mode, with Cu Kα radiation ($\lambda = 1.5418$ Å) and generator setting 40 kV and 40 mA. For **2** and **3**, gently ground powders were deposited in the hollow of a quartz zero-background plate supplied by The Gem Dugout, Swarthmore, PA. Experimental conditions: slits DS 0.5°, AS 0.5°, RS 0.1 mm; secondary beam graphite monochromator, Na(Tl)I scintillation counter; pulse-height amplifier discrimination. Data collections details: **2**, step scan mode, $5 < 2\theta < 105°$, $\Delta 2\theta = 0.02°$, $t = 16$ s step^{-1}; **3**, step scan mode, $6 < 2\theta < 75°$, $\Delta 2\theta = 0.02°$, $t = 25$ s step^{-1}. Silicon NBS 640b was used as an external standard. For **4** and **5**, gently ground powders were deposited in the hollow of a silicon zero-background plate supplied by Officina Elettrotecnica di Tenno, Ponte Arche, Italy, inserted in a temperature-controlled sample heater. Experimental conditions: slits DS 0.5°, AS 8 mm; nickel filter; linear PSD Lynxeye detector. Data collections details: **4**, continuous scan mode, $6 < 2\theta < 75°$, $\Delta 2\theta = 0.02°$, total time 16 h, $T = 115$ °C; **5**, continuous scan mode, $5 < 2\theta < 35°$, $\Delta 2\theta = 0.02°$, total time 16 h, $T = 140$ °C. A plot of the raw diffraction data for the four powder samples (**2**−**5**) is shown in Figure 1. For species **2**−**4**, standard peak search procedures were followed by indexing through the singular value decomposition method implemented in TOPAS-R.[25] For **2**, indexing of the first 24 lines ($2\theta < 20°$) allowed the determination of a triclinic cell with approximate lattice parameters $a = 10.91$, $b = 13.70$, $c = 16.04$ Å, $\alpha = 105.0°$, $\beta = 108.8°$, $\gamma = 105.1°$, $V = 2034$ Å^3, and figure of merit 18.8. Density indicated a $Z = 1$ value and $P\bar{1}$ as the probable space group. For **3**, indexing of the first 20 lines ($2\theta < 17°$) allowed the determination of a primitive monoclinic cell with approximate lattice parameters $a = 11.14$, $b = 26.61$, $c = 14.37$ Å, $\beta = 102.8°$, $V = 4154$ Å^3, and figure of merit 30.3. Systematic absences, density, and geometrical considerations indicated a $Z = 2$ value and space group $P2_1/c$. For **4**, indexing of the first 18 lines ($2\theta < 18°$) indicated a primitive monoclinic cell with approximate lattice parameters $a = 10.90$, $b = 26.41$, $c = 14.16$ Å, $\beta = 102.7°$, $V = 3978$ Å^3, and figure of merit 15.9. Also in this case, systematic absences and density considerations indicated a $Z = 2$ value and space group $P2_1/c$. For **5**, due to a much higher number of (relatively broad) lines observed already at low angles, conventional peak search and indexing methods did not suggest any plausible cell. Therefore, use was made of the brutal-force method implemented in the simulated annealing technique for whole-pattern matching (lattice-parameter search of TOPAS-R, $2\theta < 32°$), which resulted in a triclinic lattice with $a = 11.61$, $b = 25.41$, $c = 14.06$ Å, $\alpha = 91.8°$, $\beta = 108.2°$, $\gamma = 97.3°$, $V = 3901$ Å,^{3} and $R_{wp} = 0.056$. Density and geometrical considerations indicated a $Z = 2$ value and space group $P\bar{1}$. The structural models of **2**−**4**, employed in the final whole-pattern Rietveld-like refinements, were determined ab initio by the simulated annealing technique implemented in TOPAS-R, using a rigid Ni_2(dpyatriz) moiety taken from the structure of **1** (flexible

Table 1. Crystallographic Data and Refinement Details for $[Ni_4(dpyatriz)_2(NO_3)_8(CH_3CN)_2(H_2O)_2]\cdot 2CH_3CN$ (**1**)

formula	$C_{74}H_{64}N_{36}Ni_4O_{26}$
fw	2108.45
cryst syst	triclinic
space group	$P\bar{1}$
a/Å	10.7305(7)
b/Å	14.6369(9)
c/Å	15.8826(10)
α/deg	111.257(2)
β/deg	92.495(2)
γ/deg	107.521(2)
V/Å^3	*2184.0(2)*
Z	1
D_{calc}/g cm^{-3}	1.600
T/K	150(2)
λ/Å	0.6894
μ/mm^{-1}	0.949
F(000)	1080
reflcns collcd/unique	23 775/12 483 ($R_{int} = 0.022$)
final R indices [$I > 2\sigma(I)$]	R1 = 0.0567, wR2 = 0.1525
R indices (all data)	R1 = 0.0648, wR2 = 0.1592
GOF	1.037

(11) Demeshko, S.; Dechert, S.; Meyer, F. *J. Am. Chem. Soc.* **2004**, *126*, 4508−4509.
(12) de Hoog, P.; Gamez, P.; Mutikainen, H.; Turpeinen, U.; Reedijk, J. *Angew. Chem., Int. Ed.* **2004**, *43*, 5815−5817.
(13) Schottel, B. L.; Chifotides, H. T.; Shatruk, M.; Chouai, A.; Perez, L. M.; Bacsa, J.; Dunbar, K. R. *J. Am. Chem. Soc.* **2006**, *128*, 5895−5912.
(14) Mascal, M., *Angew. Chem., Int. Ed.* **2006**, *45*, 2890−2893.
(15) Quinonero, D.; Garau, C.; Rotger, C.; Frontera, A.; Ballester, P.; Costa, A.; Deya, P. M. *Angew. Chem., Int. Ed.* **2002**, *41*, 3389−3392.
(16) Kim, D.; Tarakeshwar, P.; Kim, K. S. *J. Phys. Chem. A* **2004**, *108*, 1250−1258.
(17) Casellas, H.; Gamez, P.; Reedijk, J.; Mutikainen, I.; Turpeinen, U.; Masciocchi, N.; Galli, S.; Sironi, A. *Inorg. Chem.* **2005**, *44*, 7918−7924.
(18) de Hoog, P.; Gamez, P.; Driessen, W. L.; Reedijk, J. *Tetrahedron Lett.* **2002**, *43*, 6783−6786.
(19) Seward, C.; Pang, J.; Wang, S. *Eur. J. Inorg. Chem.* **2002**, 1390−1399.
(20) Kahn, O. *Molecular Magnetism*; VCH Publishers: New York, 1993.
(21) Cernik, R. J.; Clegg, W.; Catlow, C. R. A.; BushnellWye, G.; Flaherty, J. V.; Greaves, G. N.; Burrows, I.; Tayloe, D. J.; Teat, S. J.; Hamichi, M. *J. Synchrotron Radiat.* **1997**, *4*, 279−286.
(22) *SAINT, S. a.*; SiemensAnalytical X-ray Instruments Inc.: Madison, WI.
(23) Sheldrick, G. M. *SHELXS-97 Program for Crystal Structure Determination*; University of Göttingen: Göttingen, Germany, 1997.
(24) Sheldrick, G. M. *SHELXL-97-2 Program for Crystal Structure Refinement*; University of Göttingen: Göttingen, Germany, 1997.
(25) *Topas-R General profile and structure analysis software for powder diffraction data*; Bruker AXS: Karlsruhe, Germany.

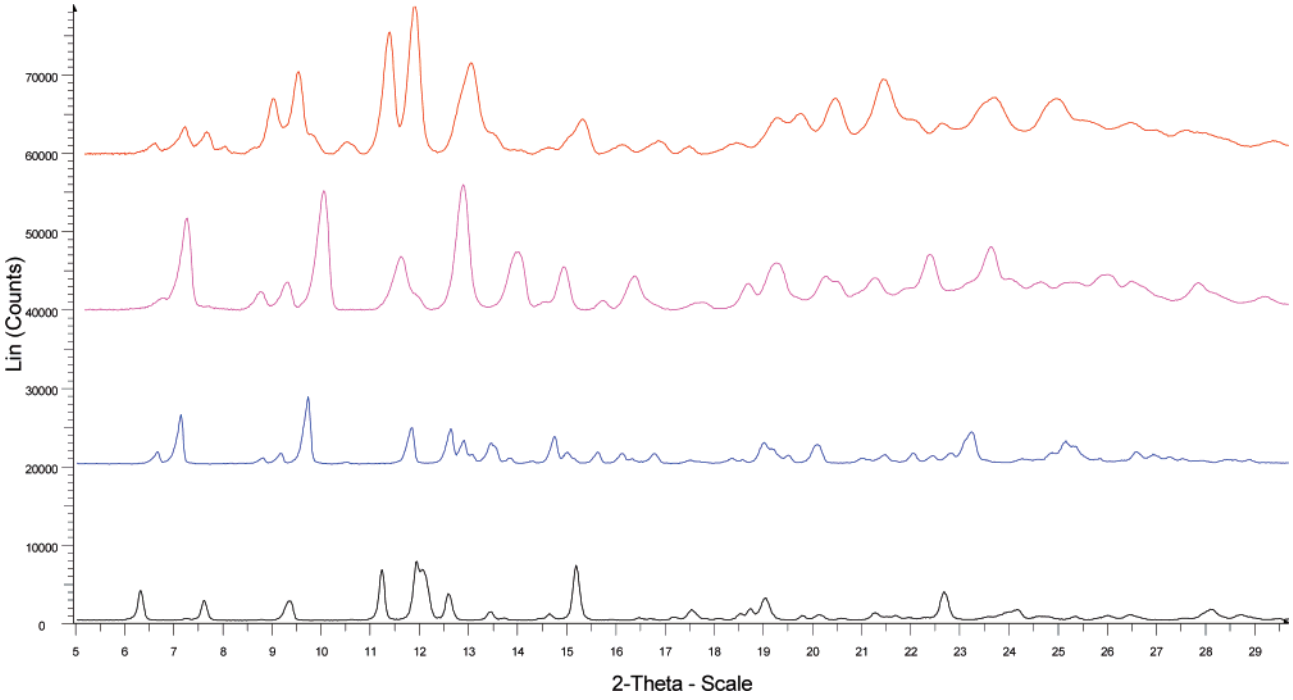

Figure 1. Raw XRPD traces for compounds **2**−**5** (bottom to top).

at the three exocyclic C−N links of the central triazine), four D_{3h} nitrate groups and, when pertinent, oxygen atoms for the coordinated and clathrated water molecules. In agreement with the crystallochemical observations gathered in the Results and Discussion (vide infra), for **2** it was assumed that all CH_3CN moieties were substituted by water molecules, maintaining the overall molecular connectivity found in **1**; for **3** and **4**, it was further assumed that reorganization of the nitrate ions (two on each Ni(II) center) had occurred, with *12* H_2O molecules (per tetranuclear complex) in the fully hydrated species **3** and *none* in the anhydrous species **4**, generated above 100 °C. Accordingly, several antibumping O···O conditions and a few Ni−O restraints, helping stability and convergence to chemically meaningful models, were included. In all three species **2**−**4**, and despite the different lattice symmetries, each tetranuclear moiety possesses crystallographically imposed $\bar{1}$ symmetry. In each case, the background contribution was modeled by a polynomial function; a preferred orientation correction was found to be necessary for species **2** and **3**, and an overall isotropic B_M value was refined. Peak shapes were described by the fundamental parameters approach. The final Rietveld refinement plots are depicted in Figure 2.

Crystal data for **2**: $C_{66}H_{60}N_{32}Ni_4O_{30}$, fw 2016.10; triclinic $P\bar{1}$; $a = 10.920(1)$, $b = 13.732(1)$, $c = 16.057(2)$ Å; $\alpha = 104.95(6)$, $\beta = 108.93(7)$, $\gamma = 105.04(1)°$; $V = 2039.6(5)$ Å^3; $Z = 1$; $\rho_{calc} = 1.641$ g cm^{-3}; $R_p = 0.14$, $R_{wp} = 0.19$ for 5001 data collected in the $5 < 2\theta < 105°$ range, $R_B = 0.097$.

Crystal data for **3**: $C_{66}H_{72}N_{32}Ni_4O_{36}$, fw 2124.18; monoclinic, $P2_1/c$; $a = 11.120(1)$, $b = 26.549(3)$, $c = 14.346(2)$ Å; $\beta = 102.762(8)°$; $V = 4130.7(8)$ Å^3; $Z = 2$; $\rho_{calc} = 1.534$ g cm^{-3}; $R_p = 0.06$, $R_{wp} = 0.18$ for 3451 data collected in the $6 < 2\theta < 75°$ range, $R_B = 0.088$.

Crystal data for **4**: $C_{66}H_{48}N_{32}Ni_4O_{24}$, fw 1908.02; monoclinic, $P2_1/c$; $a = 11.033(2)$, $b = 26.192(4)$, $c = 13.910(2)$ Å; $\beta = 99.38(1)°$; $V = 3966(1)$ Å^3; $Z = 2$; $\rho_{calc} = 1.778$ g cm^{-3}; $R_p = 0.06$, $R_{wp} = 0.10$ for 3451 data collected in the $6 < 2\theta < 75°$ range at 115 °C, $R_B = 0.047$.

Crystallographic data for **1**−**4** have been deposited with the Cambridge Crystallographic Data Centre as supplementary publication Nos. CCDC 634834 (**1**) and 634929−634931 (**2**−**4**).

No attempt in solving the structure of **5** was performed, since its complexity, manifested by the nature of the measured XRPD trace and by the (triclinic) lattice parameters derived from it, falls well beyond the capabilities of the methods. However, it can be easily recognized that the monoclinic cell of **4** and the triclinic one of **5** share very similar features, that of **5** being just a lower symmetry version of the monoclinic one. Therefore, it is likely that the molecular structural model in **5** is very similar to that of **4**, with the notable absence of the crystallographic inversion center relating two halves of the tetranuclear complex. For the sake of completeness, it should be noted that this lowering of crystal symmetry can also be obtained by packing, in $P\bar{1}$, two (slightly) different centrosymmetric molecules, each lying on distinct crystallographic inversion centers. Whether the former or the latter structural hypothesis is true, however, cannot be solved from state-of-the-art powder diffraction methods.

Crystal data for **5**: $C_{66}H_{48}N_{32}Ni_4O_{24}$, fw 1908.02; triclinic $P\bar{1}$; $a = 11.581(4)$, $b = 25.546(9)$, $c = 14.100(5)$ Å; $\alpha = 91.64(1)$, $\beta = 108.17(1)$, $\gamma = 97.37(1)°$; $V = 3920(2)$ Å^3; $Z = 2$; $\rho_{calc} = 1.616$ g cm^{-3}; $R_{wp} = 0.047$ (structureless Le Bail fit) for 1501 data collected in the $5 < 2\theta < 35°$ range at 140 °C.

Thermodiffractometric experiments were performed in air in the 20−160 °C range using a custom-made sample heater with nominal ±0.1 °C stability, assembled by Officina Elettrotecnica di Tenno, Ponte Arche, Italy. A small sample of compound **3** was heated in 5 °C steps and its XRPD trace recorded. The evolution of the lattice parameters, determined by the structureless Le-Bail method, allowed the estimation of the structural changes later discussed, i.e., the (negative) thermal expansion coefficients and of the **3** to **4** phase change occurring above 110 °C. Further heating above 130 °C showed splitting of most peaks of **4** and formation of a triclinic phase (compound **5**). On cooling to RT (room temperature) in air, species **3** is restored without the intermediate formation of species

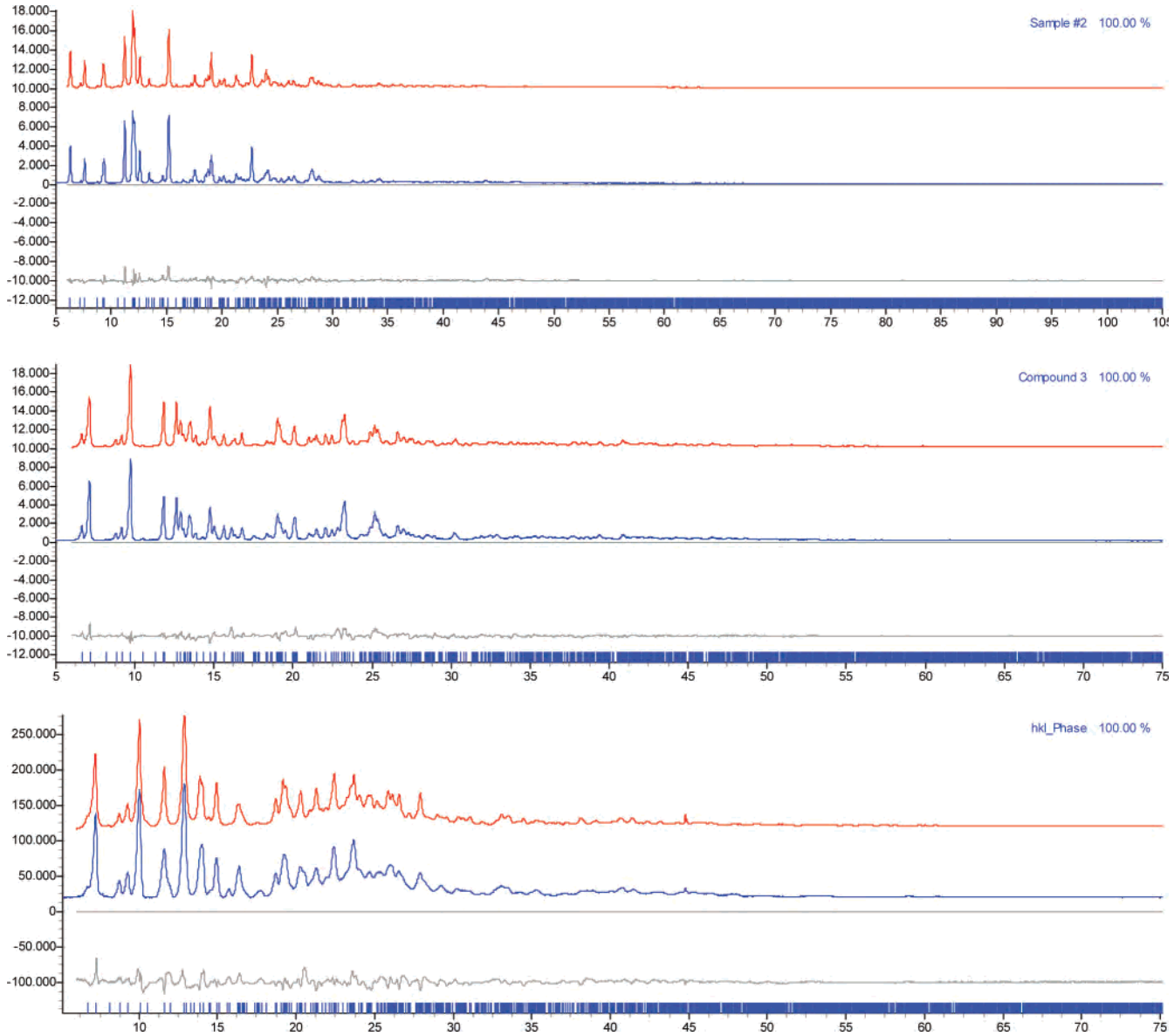

Figure 2. Final Rietveld refinement results, in terms of experimental (blue), calculated (red), and difference (gray) plots, and peak markers at the bottom. Top to bottom: compounds **2**−**4**. Horizontal axis: 2θ, deg. Vertical axis: intensity, counts.

4. So, species **4** is a *metastable* phase that can only be generated under kinetic control when desorbing *all* water molecules from **3**.

Results and Discussion

Synthesis and Spectroscopy. The reaction of the polydentate triazine-based dpyatriz ligand (Chart 1) with nickel(II) nitrate using a solvothermal procedure in acetonitrile yields a tetranuclear complex formulated as $[Ni_4(dpyatriz)_2(NO_3)_8(H_2O)_2(CH_3CN)_2]\cdot 2CH_3CN$ (**1**). **1** crystallizes as blue nearly cubic microcrystals, which, in contact with air moisture, rapidly undergo an irreversible transformation to give a blue-gray crystalline (XRPD evidence) powder, **2**. A prolonged exposition of **2** to moisture produces another pseudopolymorphic phase, **3**, as discussed below (see XRPD Analyses).

Owing to its high moisture sensitivity, spectral and analytical data could not be obtained for **1**. Actually, the IR and ligand-field spectra characterize a hydrated phase, whose elemental analyses point toward a compound of $[Ni_4(dpyatriz)_2(NO_3)_8(H_2O)_{12}]$ formula, namely the stable pseudopolymorph **3**. As clarified in the following section, **3** is obtained through the formation of the metastable compound **2**, i.e., $[Ni_4(dpyatriz)_2(NO_3)_8(H_2O)_6]$, upon exposure to ambient humidity. The IR spectrum of **3** evidences the coordination of all pyridine units of the dpyatriz ligand. Indeed, the band corresponding to the pyridine ring bending vibration mode is observed at 1024 cm^{-1}. For the free ligand, this band is detected at 995 cm^{-1}, which is not present in the spectrum of the complex. The electronic diffuse reflectance spectrum of **3** exhibits two main features: the presence of three broad bands centered at 589, 453, and 381 nm; a more intense absorption band at 275 nm. The broad signals are assigned to spin-allowed d−d transitions, namely $^3A_{2g} \rightarrow {}^3T_{1g}$ and $^3A_{2g} \rightarrow {}^3T_{1g}(P)$.[26] The three absorption bands observed in

(26) Sun, Y. J.; Shen, W. Z.; Cheng, P.; Yan, S. P.; Liao, D. Z.; Jiang, Z. H.; Shen, P. W. *Polyhedron* **2004**, *23*, 211−218.

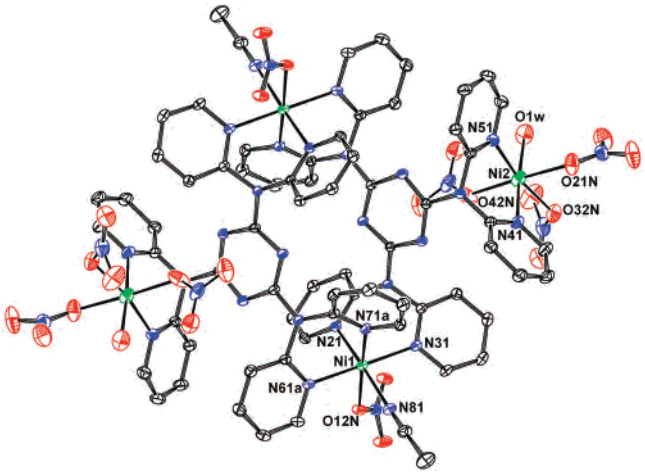

Figure 3. ORTEP[27] view of $[Ni_4(dpyatriz)_2(NO_3)_8(CH_3CN)_2(H_2O)_2]$ (displacement ellipsoids drawn at 30% probability level). Hydrogen atoms are omitted for clarity. Symmetry operation for equivalent atoms, a: $-x + 2, -y + 1, -z + 1$.

Table 2. Selected Bond Lengths (Å) and Angles (deg) for $[Ni_4(dpyatriz)_2(NO_3)_8(CH_3CN)_2(H_2O)_2]\cdot 2CH_3CN$ (**1**)

bond dists for Ni1		bond dists for Ni2	
Ni1−N21	2.075(2)	Ni2−N41	2.087(2)
Ni1−N31	2.075(2)	Ni2−N51	2.077(2)
Ni1−N61a	2.077(2)	Ni2−O21N	2.091(3)
Ni1−N71a	2.092(2)	Ni2−O32N	2.078(5)
Ni1−N81	2.136(2)	Ni2−O42N	2.046(3)
Ni1−O12N	2.088(2)	Ni2−O1W	2.067(3)

angles for Ni1		angles for Ni2	
N31−Ni1−N71a	90.67(7)	N41−Ni2−N51	89.21(9)
N71a−Ni1−N61a	87.44(7)	N51−Ni2−O1W	90.50(11)
N61a−Ni1−O12N	88.70(7)	O1W−Ni2−O32N	88.5(2)
O12N−Ni1−N31	93.07(7)	O32N−Ni2−N41	90.99(18)
N21−Ni1−N81	174.17(8)	O21N−Ni2−O42N	176.60(11)

the 380−600 nm region are thus indicative of the existence of two types of hexacoordinated Ni^{II} chromophores in octahedral environments (since the $^3A_{2g} \rightarrow {}^3T_{1g}$ absorption is split in two maxima, namely 453 and 381 nm), most likely as a result of the two different N_2O_4 and N_4O_2 donor sets (as observed in the crystal structure of **1** but taking into account that the molecules of acetonitrile of **1** have been replaced by water molecules in **3**). The intense signal at 275 nm is attributed to a ligand to metal charge-transfer transition.

Crystal and Molecular Structure of 1. An ORTEP[27] view of the tetranuclear $[Ni_4(dpyatriz)_2(NO_3)_8(H_2O)_2(CH_3CN)_2]\cdot 2CH_3CN$ (**1**) is depicted in Figure 3. Selected bond distances and angles are presented in Table 2. **1** crystallizes in the centrosymmetric triclinic *P-1* space group. The two metal centers Ni1 and Ni2 of the asymmetric unit are hexacoordinated in octahedral geometry. The coordination environment of Ni1 includes four nitrogen atoms of two bidentate dipyridylamine units belonging to two different dpyatriz ligands [Ni1−N21 2.075(2); Ni1−N31 2.075(2); Ni1−N61a 2.077(2); Ni1−N71a 2.092(2) Å] (symmetry operation for equivalent atoms a: $-x + 2, -y + 1, -z + 1$), one oxygen atom of a monodentate nitrate anion [Ni1−O12N 2.088(2) Å], and one nitrogen atom of an acetonitrile molecule [Ni1−N81 2.136(2) Å]. The atoms N61a, O12N, N31, and N71a define the basal plane of the octahedron, while the atoms N21a and N81 are located at the axial positions. The bond distances, as well as the basal angles, ranging from 87.44(7) to 93.07(7)°, can be considered as normal.[28] Ni2 is also in an octahedral coordination environment arising from one N-bidentate dipyridylamine unit [Ni2−N51 2.077(2); Ni2−N41 2.087(2) Å], one O-monodentate nitrate anion [Ni2−O32N 2.078(5) Å], and one water molecule [Ni2−O1W 2.067(3) Å] at the basal plane and two O-monodentate nitrate anions [Ni2−O21N 2.091(3); Ni2−O42N 2.046(3) Å] occupying the axial positions. The bond distances, as well as the basal angles, varying from 88.5(2) to 90.99(2)°, are in the normal range for octahedral NiN_2O_4 chromophores.[29]

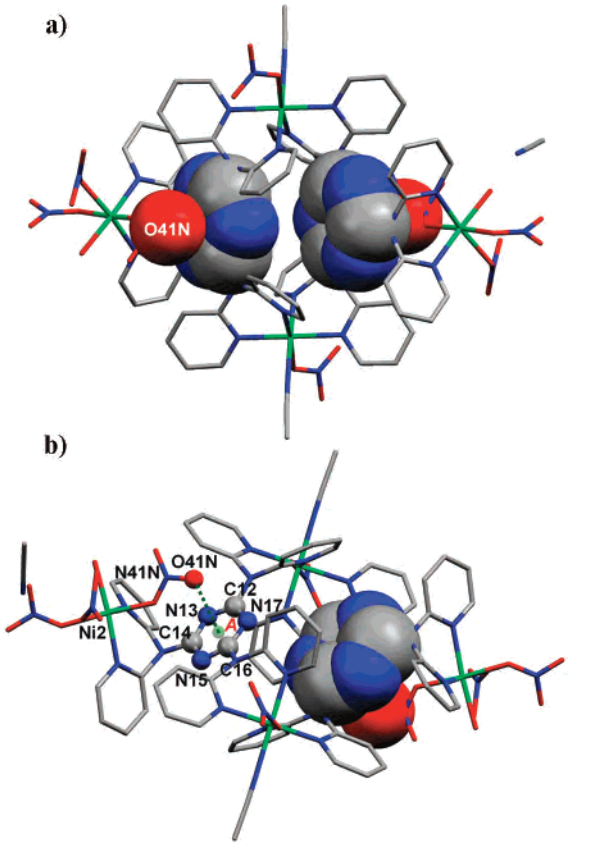

Figure 4. Anion−*s*-triazine interactions[33] in **1**: (a) top view; (b) side view, showing the interaction between the oxygen atom O41N of a coordinated nitrate and the 1,3,5-triazine ring (O41N···centroid A of 3.238 Å).

As anticipated from earlier theoretical and crystallographic evidence,[30] **1** exhibits an unusual supramolecular feature, that is, the occurrence of anion binding interactions between nitrate anions and triazine rings. The atoms N41N and O41N of a nitrate anion coordinated to Ni2 are indeed involved in strong interactions with the adjacent triazine ring (Figure 4). Such nitrate−triazine interactions have been recently encountered in zinc(II) complexes with a related ligand, namely

(27) Spek, A. L. *Platon, A Multipurpose Crystallographic Tool*; Utrecht University: Utrecht, The Netherlands, 2006.

(28) Berlinguette, C. P.; Galan-Mascaros, J. R.; Dunbar, K. R. *Inorg. Chem.* **2003**, *42*, 3416−3422.

(29) Noveron, J. C.; Lah, M. S.; Del Sesto, R. E.; Arif, A. M.; Miller, J. S.; Stang, P. J. *J. Am. Chem. Soc.* **2002**, *124*, 6613−6625.

(30) Casellas, H.; Massera, C.; Buda, F.; Gamez, P.; Reedijk, J. *New J. Chem.* **2006**, *30*, 1561−1566.

Table 3. Distances (Å) between the Coordinated Nitrate and the *s*-Triazine Ring Reflecting Their Reciprocal Binding Interactions Existing in **1** (Figure 4b)

O41N···N17	3.141(5)	O41N···C14	3.814(5)
O41N···C16	3.229(5)	N41N···N13	3.462(6)
O41N···C12	3.336(5)	N41N···C14	3.494(6)
O41N···N15	3.691(5)	N41N···N15	3.709(7)
O41N···N13	3.734(5)		

2,4,6-tris(di-2-picolylamino)-1,3,5-triazine (dipicatriz).[31] The oxygen atom O41N is in close contact with the nitrogen atom N17 of the triazine ring (O41N···N7 3.141(5) Å). Nearly all distances between this nitrate oxygen and the atoms of the electron-poor aromatic ring (Table 3) are below the 3.8 Å value[32] and are indicative of a significant interaction. These short contacts give rise to a centroid···O41N distance of only 3.238 Å (Figure 4); moreover, as shown in Table 3, also the nitrogen atom N41N of this nitrate anion shows relatively short contacts with the triazine unit.

X-ray Powder Diffraction Studies: Pseudopolymorphism. The experimental XRPD traces of compounds **2**−**5** are collectively shown in Figure 1. Species **1**, $[Ni_4(dipyatriz)_2(NO_3)_8(H_2O)_2(CH_3CN)_2]\cdot 2CH_3CN$, is stable only under an excess of acetonitrile. As soon as it is exposed to ambient conditions, it loses its shiny luster, turning opaque, but maintaining (poly)crystallinity. Single crystals of **1** are destroyed upon loss of CH_3CN molecules; their X-ray powder diffraction trace transforms within minutes from that expected for **1** into a new pattern, that of **2**, $[Ni_4(dipyatriz)_2(NO_3)_8(H_2O)_4]\cdot 2H_2O$, a polyhydrated species. As monitored by XRPD, addition of a few drops of CH_3CN from the mother liquor on top of the powders of **2** promotes the formation of a solvated phase (**1$_X$**), not isomorphous to **1**, which can be formulated as $[Ni_4(dipyatriz)_2(NO_3)_8(H_2O)_x(CH_3CN)_y]$. Obviously, having sucked water molecules from the environment, compound **2**, upon exposure to CH_3CN, cannot restore **1** but only affords the elusive **1$_X$** species (see Chart 2). At room temperature, in air, **1$_X$** loses the acquired solvent in about 5 min, restoring **2**. The limited ($2\theta < 15°$) XRPD dataset of **1$_X$**, collected under the mother liquor, showed a systematic shift of some peaks toward low angles with respect to those of **2**, consistent with a (tentative) unit cell of $a = 10.45$, $b = 13.74$, $c = 16.63$ Å, $\alpha = 108.8$, $\beta = 103.0$, $\gamma = 100.1°$, $V = 2123$ Å^3, and $Z = 1$, i.e., that of a slightly expanded phase **2**.

Compound **2** is stable for several hours at room temperature in the diffractometer chamber, allowing the collection of meaningful diffraction data with sufficient counting statistics for a structural analysis. Yet, **2** was found to transform if left in air for several days. The new XRPD trace was initially attributed to species **3**, $[Ni_4(dipyatriz)_2(NO_3)_8(H_2O)_4]\cdot 8H_2O$, which was later confirmed by repeatedly preparing this phase upon exposing **2** (or **1**) to a moist air at room temperature for 18 h. If heated in situ by an accurate temperature-controlled hot-stage, species **3** shows a systematic variation of the peaks positions, of *opposite* sign to what

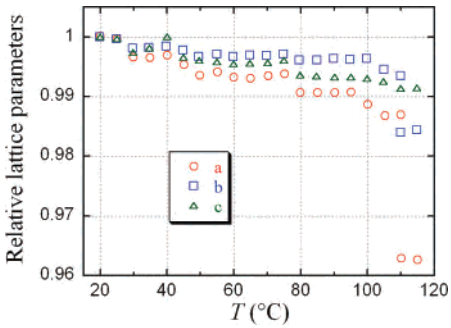

Figure 5. Evolution of the relative lattice parameters (in the x/x_0 form) of species **3** on increasing the sample temperature in the 20−120 °C range. Note the smooth decrease of *all* axes vs *T* and the sudden jump of *a* and *b* (*but not c*) at about 110 °C.

would be expected for thermal expansion of molecular species (with $\partial \ln V/\partial T$ of the order of 10^{-5} K^{-1}). Figure 5 shows the temperature dependence of the lattice parameters in the 20−120 °C range, from which the $\partial \ln a/\partial T = -1.0 \times 10^{-4}$, $\partial \ln b/\partial T = -4.3 \times 10^{-5}$, and $\partial \ln c/\partial T = -8.6 \times 10^{-5}$ K^{-1} (thus $\partial \ln V/\partial T = -2.5 \times 10^{-4}$ K^{-1}) coefficients can be derived. These numbers unequivocally indicate that water molecules are lost in a rather continuous manner up to ca. 100 °C, above which the anhydrous α-$[Ni_4(dipyatriz)_2(NO_3)_8]$ phase (**4**) is formed. This last transformation is associated with a noticeable shrinking of the molar volume and is fully reversible, although rehydration is a much slower process and occurs within a measurable amount of time (minutes) only below ca. 75 °C. Interestingly, the water loss from **3** does not restore species **2** as an intermediate phase (before complete dehydration to **4**), thus suggesting that compounds **2** and **3** possess a slightly different structure or connectivity (vide infra).

If compound **4** is heated above 135 °C, a further change in the diffraction trace is observed, which has been interpreted as a molecular rearrangement involving dissymmetrization (from $P2_1/c$ into $P\bar{1}$, maintaining similar metrics), without significant structural changes or partial decomposition, to give β-$[Ni_4(dipyatriz)_2(NO_3)_8]$, **5**. The slightly lower molar volume of **5** with respect to that of **4** suggests that the thermodynamically stable polymorph is indeed complex **5** and that **4** is a relative minimum in the **3** → **4** → **5** path. This hypothesis is further substantiated by the *direct* formation of **3** in air on cooling species **5**, without any detectable amount of **4**.

Crystal and Molecular Structures of 2−4. The structural models for the complex species **2**−**4** have been derived from X-ray powder diffraction data on less-than-ideal polycrystalline samples of a rather high structural complexity, well beyond that commonly tackled with state-of-the-art software and laboratory instruments. Accordingly, the models presented here, suffering from heavy idealization or hidden assumptions, do not possess, more than ever, the quality of those derived from single-crystal methods and should be considered only moderate approximations to reality. Thus, the discussion below mainly addresses the local connectivity at the metal atoms, highlighted in the sketches of the molecular structures of **2** and **4** shown in Figure 6.

(31) Maheswari, P. U.; Modec, B.; Pevec, A.; Kozlevcar, B.; Massera, C.; Gamez, P.; Reedijk, J. *Inorg. Chem.* **2006**, *45*, 6637−6645.
(32) Janiak, C. *Dalton Trans.* **2000**, 3885−3896.
(33) Mooibroek, T. J.; Gamez, P. *Inorg. Chim. Acta* **2007**, *360*, 381−404.

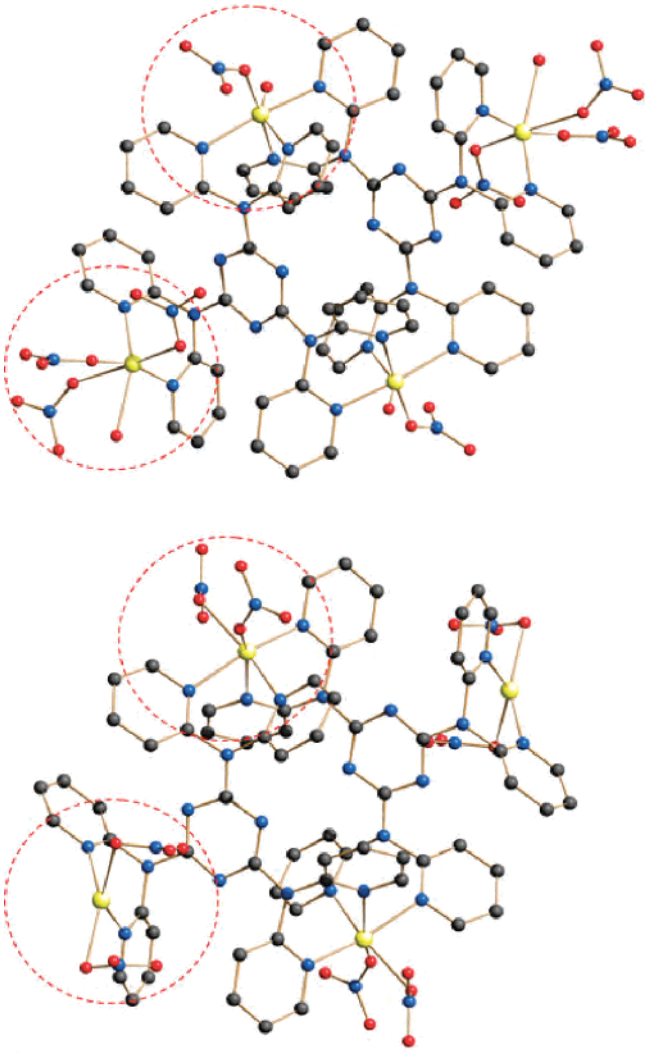

Figure 6. Schematic drawing of the molecular structures of compounds **2** (top) and **4**. Note the similarity of the molecular core and the different coordination (highlighted) at the nickel atoms: $NiN_4(NO_3)(H_2O)/NiN_2(NO_3)(H_2O)_3$ and $NiN_4(NO_3)_2/NiN_2(NO_3)_2$, respectively.

The homogeneous lattice metrics of species **1**−**5**, synoptically collected in Table 4, and the easy and fast interconversion among many of these phases by simple exposure to moisture or moderate heat, clearly indicate that the overall structure of the tetranuclear complex is only weakly perturbed during the (pseudo)polymorphic transformations. For example, in **2**, substitution of the coordinated acetonitrile molecules by water ones leads to two different chromophores, of the $NiN_2(NO_3)_3(H_2O)$ and $NiN_4(NO_3)(H_2O)$ type, maintaining the inner $[Ni_4(dipyatriz)_2]$ skeleton virtually unchanged.

As anticipated above, **2** transforms into **3** at RT in a moist environment, but this transformation is not reversible. This fact suggests that not only additional water molecules are sucked into the lattice but also a slightly more pronounced (water mediated?) structural rearrangement occurs (as corroborated by the crystal symmetry change and doubling of the *b* axis). Likely, and driven by redistribution of the anionic ligands onto the different metal ions, the $NiN_2(NO_3)_2(H_2O)_2$ and $NiN_4(NO_3)_2$ chromophores are formed, the remaining water molecules being hosted in new cavities of the slightly expanded lattice (see Table 3).

These water molecules are progressively released upon gentle heating, until an anhydrous phase forms above 110 °C, α-$[Ni_4(dipyatriz)_2(NO_3)_8]$, probably containing chelating nitrates when the coordinated water molecules are lost. A true polymorph of **4**, the *β* phase, forms at slightly higher temperatures. The negligible change of the color and hue of these specimens during all these transformations speaks for a constancy, or similarity, of the crystal field strengths about the nickel(II) ions and, therefore, excludes the occurrence of square-planar (yellow) or tetrahedral (deep blue) NiX_4 geometries. This observation is apparently in contrast with the proposed location and connectivity of the nitrate ligands shown in Figure 6 for species **4** (for a possible reconciling explanation, see the following paragraph). In addition, the easy **3** → **4** → **5** → **3** cyclic transformation, described above, speaks for the presence of nearly identical complexes in slightly different crystalline environments.

The crystal structure analyses discussed above suffer from a number of unavoidable problems, which simultaneously affect the quality and reliability of the proposed results: first of all, the complexity of the molecular species, which powder diffraction methods *alone* cannot handle; second, fragmentation and formation of small coherent domains, or even disorder or ligand dynamics introduced by solid-state reactions, as well as thermal treatment and recycling of these soft materials; finally, the experimental setup for high-temperature measurements, which inherently generates instrumental (optical and geometrical) aberrations. Thus, apart from the identity of the (water or nitrate) ligands about each nickel ion, neither quantitative geometrical features nor details of the true coordination at each metal could be derived.

Table 4. Synoptic Collection of Crystal Data for Species **1**−**5**, Highlighting the Strict Metric (and Structural) Relationships Existing among Them[a]

species	*T*/K	space group	*a*/Å	*b*/Å	*c*/Å	α/deg	*β*/deg	*γ*/deg	*Z*	(*V*/*Z*)[a]/Å^3	solv mol/*Z*[b]	empty (*V*/*Z*)[c]/Å^3	packing coeff
1	150	$P\bar{1}$	10.730	14.636	15.883	111.26	92.49	107.52	1	2184 (1399)	2 + 2[d] + 2[d]	53 (200)	0.68
$\mathbf{1_X}$	298	$P\bar{1}$	10.45	13.74	16.63	108.8	103.0	100.1	1	2123 (na)	na	na	na
2	298	$P\bar{1}$	10.920	13.732	16.057	104.95	108.93	105.04	1	2040 (1341)	**4** + 2	52 (112)	0.67
3	*298*	$P2_1/c$	11.120	26.549	14.346	90	102.76	90	2	2065 (1299)	**4** + 8	0 (133)	0.69
4	*388*	$P2_1/c$	11.033	26.192	13.910	90	99.38	90	2	1983 (1296)	**0** + 0	100	0.65
5	413	$P\bar{1}$	11.581	25.546	14.100	91.64	108.17	97.37	2	1960 (na)	**0** + 0	na	na

[a] Ideally, **1**, $\mathbf{1_X}$, and **2** transform into **3**−**5** by doubling of the *b* axis. Standard deviations for the cell parameters can be found in the Experimental Section presented above. [b] Molecular volume in parentheses. [c] Number of directly bonded solvent molecules in bold. [d] Empty volume upon removing the clathrated solvent in parentheses. [e] CH_3CN. These estimates have been calculated with SMILE (Eufri, D.; Sironi, A. *J. Mol. Graphics* **1989**, *7*, 165−169).

However, supramolecular structural features are less affected by the intrinsic loss of details inherent in our crystallographic data analysis; this allows meaningful crystal packing analyses, which coherently supply missing structural information to the blurry picture presented above. The $[Ni_4(dpyatriz)_2(NO_3)_8(L)_4]$ ($L = H_2O$ or CH_3CN) and $[Ni_4(dpyatriz)_2(NO_3)_8]$ moieties of **1**−**5** share some common features, such as their centrosymmetric nature, discoidal (oblate) shape, and global packing arrangement. However, on doubling the *b* axis as in species **3** and **4**, their enclosure cell slightly changes: indeed, in the latter compounds, the neighboring molecules along *b* are generated by the 2_1 axis rather than by a simple lattice translation. Reasonably, the same packing is maintained in **5** where the decrease in symmetry (and the loss of the 2_1 axis) is compensated by the presence of a new independent "molecule". The substantial similarity of the overall packing in **1**−**5** on varying the kind and number of bound and clathrated "solvent" molecules is reflected in substantial relative variation of molecular volumes and packing coefficients. From the data in Table 3 (packing coefficients, empty *V*/*Z*, and molecular volumes), it is clear that compound **3** is the most compact, thus corroborating the observation of its spontaneous formation from the metastable phase **2**.

Conclusions

In this paper, we have presented the reaction of nickel(II) nitrate with the dpyatriz ligand in acetonitrile, which yields tiny- crystals of $[Ni_4(dpyatriz)_2(NO_3)_8(CH_3CN)_2(H_2O)_2]\cdot 2CH_3CN$formula (**1**), structurally characterized by X-ray diffraction using a synchrotron radiation source; **1** exhibits remarkable anion$\cdots\pi$ interactions between the coordinated nitrate ions and the electron poor triazine rings. Amazingly, the compound is not stable in ambient conditions yet, through a number of solvent exchange and dehydration processes, it can be easily transformed into a number of pseudopolymorphic phases (**2**−**5**), all containing a practically unchanged $[Ni_4(dpyatriz)_2]$ core.

The interconversion scheme among the different polymorphs has been determined by using controlled heating, and their basic structural features have been assessed through ab initio X-ray powder diffraction methods. In these complex cases, the quality of the final image reconstructed from powder diffraction data cannot be compared to that attainable from conventional single-crystal structural analyses. Many factors (see above) concur to lower the resolution of the final model, as it is customary observed for protein diffraction methods, where topologies and conformations, rather than accurate bond distances and angles, are derived.

Acknowledgment. This work has been financially supported by the Graduate Research School Combination "Catalysis", a joint activity of the graduate research schools NIOK, HRSMC, and PTN. Financial support from COST Action D35, the Coordination by the FP6 Network of Excellence "Magmanet" (Contract No. 515767), and MIUR (PRIN2006: "Materiali Ibridi Metallo-Organici Multifunzionali con Leganti Poliazotati") is kindly acknowledged. We acknowledge the provision of time on the Small Molecule Crystallography Service at the CCLRC Daresbury Laboratory via support by the European Community-Research Infrastructure Action under the FP6 "Structuring the European Research Area" Programme (through the Integrated Infrastructure Initiative "Integrating Activity on Synchrotron and Free Electron Laser Science").

IC0702015